Optimizing telescoped heterogeneous catalysis with noise-resilient multi-objective Bayesian optimization

Guihua Luo[1], Xilin Yang[1], Weike Su[1], Tingting Qi[1], Qilin Xu[1,2], and An Su[3]*

[1] Key Laboratory of Pharmaceutical Engineering of Zhejiang Province, Collaborative Innovation Center of Yangtze River Delta Region Green Pharmaceuticals, Zhejiang University of Technology, Hangzhou, 310014, P. R. China

[2]School of Biological and Pharmaceutical Engineering, West Anhui University, Luan 237000, P. R. China

[3]College of Chemical Engineering, Zhejiang University of Technology, Hangzhou 310014, P. R. China

Email:

An Su - ansu@zjut.edu.cn

* Corresponding author

Abstract

This study evaluates the noise resilience of multi-objective Bayesian optimization (MOBO) algorithms in chemical synthesis, an aspect critical for processes like telescoped reactions and heterogeneous catalysis but seldom systematically assessed. Through simulation experiments on amidation, acylation, and SNAr reactions under varying noise levels, we identify the qNEHVI acquisition function as notably proficient in handling noise. Subsequently, qNEHVI is employed to optimize a two-step heterogeneous catalysis for the continuous-flow synthesis of hexafluoroisopropanol. Achieving considerable optimization within just 20 experimental runs, we report an E-factor of 0.3744 and a conversion rate of 76.20%, with optimal conditions set at 5.00 sccm and 35.00℃ for the first step, and 80.00 sccm and 170℃ for the second. This research highlights qNEHVI's potential in noisy multi-objective optimization and its practical utility in refining complex synthesis processes.

Keywords

Bayesian optimization; machine learning; telescoped synthesis; heterogeneous catalysis; hexafluoroisopropanol

Introduction

Chemists have long depended on their intuition and expertise to optimize chemical reactions, which is a complex task evaluating parameters including reactant concentration, residence time, and reaction temperature[1]. Bayesian optimization has become a popular and effective method in recent years[2-4], which strikes a balance between exploration and exploitation and efficiently reaches global optimum[4-6]. Meanwhile, the capability of multi-objective Bayesian optimization (MOBO) facilitates the optimization of complex multidimensional problems that involve competing objectives (such as space-time yield and E-factor)[7-10]. MOBO applied to chemical reaction optimization can search large new parameter spaces more efficiently than humans. In addition, these algorithms use only the minimum number of experiments but gain the most experimental information, making their application in the pharmaceutical industry attractive[11].

The optimization of multistep chemical syntheses is critical for the rapid development of new pharmaceuticals, as they minimize the number of intermediate purification steps and the use of solvents[12]. However, the optimization of telescoping reactions is a very time-consuming and labor-intensive task. Concatenating multiple reaction steps must consider the negative impact of intermediates on the next step (e.g., by-products, catalyst toxicity). Therefore, multistep synthesis of all variables has to be optimized simultaneously. Simultaneous optimization of the entire reaction system can reduce the number of optimization variables and decrease the time and cost of separating

intermediate products[13]. Lapkin et al. applied MOBO to synthesize p-cymene hydrocarbons from crude sulfated turpentine to maximize conversion and selectivity[14]. Kappe et al. successfully optimized the application of a two-step synthesis (imine formation-cyclization) of edaravone using MOBO[15]. However, there is little literature on MOBO in multistep heterogeneous response optimization, which is an even more complex problem.

Heterogeneous catalysis is one of the most valuable synthetic processes, and kinetic modeling is one of the traditional methods for optimizing this process[16-18]. However, the tedious process of eliminating internal and external mass transfer and determining residence time limits the efficiency and accuracy of kinetic modeling. In addition, experimental results of heterogeneous catalysis often come with noise introduced by temperature, barometric pressure, and other environmental factors, which may lead to lower search efficiency and convergence properties in the optimization[19]. Our previously developed MOBO platform[20] used NEHVI, a MOBO acquisition function for hypervolume maximization in both noisy and noise-free environments[21], but the comparison of different acquisition functions in terms of their ability to handle noise has not been systematically studied.

In this work, we first compared the noise-handling ability of four MOBO acquisition functions in optimizing three reactions at different experimental noise levels. Previously developed kinetic models of these reactions were used to simulate noisy

experimental results. Then, the acquisition function that handles the noise best was applied to a wet-lab telescoped synthesis of HFIP (hexafluoroisopropanol), where the first step involves a gas-liquid two-phase catalysis and the second step involves a gas-liquid-solid three-phase catalysis.

Experimental

Gaussian Processes. In Bayesian optimization, Gaussian Processes (GPs) are an effective surrogate model for guiding the search for the optimum of the expensive-to-evaluate objective function. By utilizing GPs, Bayesian optimization strikes a balance between exploring the unknown region and exploiting the known region of high payoffs to efficiently explore the parameter space[22]. Using the Matérn class[23] (Eq. 1) as a kernel in GP, the smoothness of the model can be adjusted to fit the characteristics of the objective function.

$$k(x, x') := \sigma_f^2 \frac{2^{1-\nu}}{\Gamma(\nu)} \left(\sqrt{2\nu} r\right)^{\nu} K_{\nu} \left(\sqrt{2\nu} r\right) \quad (1)$$

where σ_f^2 is the output variance, r is a weighted Euclidean distance, ν is non-negative parameters, K_ν is the modified Bessel function, Γ is the gamma function.

Acquisition functions for MOBO. Expected Hypervolume Improvement (EHVI) (Eq. 2) is used to select assessment points by estimating the expected increase in the hypervolume of a known Pareto front after incorporating the new point(s)[24]. The hypervolume is a measure of the space covered by the Pareto front in the objective space, and improving it means finding better a tradeoff between the objectives. Noisy expected hypervolume improvement (NEHVI) (Eq. 3) is a variation of EHVI designed

to deal with noise in the evaluation of objective functions[21]. It takes into account the uncertainty in the objective measurements and provides a more robust approach to optimization under noisy conditions. The "q" prefix in qEHVI and qNEHVI indicates that the acquisition function is intended to suggest a batch of points to be evaluated in each iteration. When q is set to 1, only a single point is suggested.

$$\alpha_{qEHVI}\left(\chi_{cand}\right)=\mathrm{E}\left[HVI\left(f\left(\chi_{cand}\right)\right)\right] \tag{2}$$

$$\alpha_{qNEHVI}\left(\chi_{cand}\right)=\frac{1}{N}\sum_{t=1}^{N}HVI\left(\tilde{f}\left(\chi_{cand}\right)|P_t\right) \tag{3}$$

Where χ_{cand} is the candidate sample, HVI is the hypervolume improvement, P_t is the Pareto front, f is the Black-box objective function, $\tilde{f}$ is the sampling function, N is the number of samples.

TSEMO is an algorithm that approximates Pareto sets using a limited number of function-valued approximations (Eq. 4)[25]. It extends the Thompson Sampling (TS) method, traditionally used for multi-armed bandit problems, to the field of continuous multi-objective optimization. TSEMO allows for efficient exploration and utilization of the solution space in problems involving multiple conflicting objectives, taking advantage of the Thompson Sampling method to balance the trade-offs inherent in multi-objective optimization tasks.

$$\text{minimize}_{x\in\chi\subseteq\mathbb{R}^d}G\left(x\right)=\left[g_1\left(x\right),g_2\left(x\right),...,g_m\left(x\right)\right] \tag{4}$$

where χ is the design space, x is the decision vector, and G is a vector of m scalar objectives $g_i\,(\boldsymbol{x})$ to be minimized.

ParEGO[26] is an extension of Efficient Global Optimization (EGO) framework. It addresses complex multi-objective optimization problems by employing an initialized

weight vector k, in conjunction with the augmented Tchebycheff function for secularization. This methodology effectively aggregates the multiple objectives into a singular optimization challenge. By sequentially extracting individual objectives and utilizing the Expected Improvement (EI) as the selection criterion, ParEGO systematically identifies the subsequent candidate solution, thereby streamlining the process of navigating through expensive multi-objective optimization landscapes.

The uniformly distributed weight vector k in ParEGO is defined as:

$$\wedge = \left\{ \lambda = \left(\lambda_1, \lambda_2, ..., \lambda_3\right) | \sum_{j=1}^{k} \lambda_j = 1 \wedge \forall j, \lambda_j = \frac{l}{s}, l \in \left\{0, ..., s\right\} \right\} \quad (5)$$

With $\left|\wedge\right| = \binom{s+k-1}{k-1}$. s determines the total number of vectors, and the scalar cost of the solution is calculated using the Tchebycheff function.

$$f_\lambda\left(x\right) = \max_{j=1}^{k}\left(\lambda_j . f_i\left(x\right)\right) + \rho \sum_{j=1}^{k} \lambda_j f_i\left(x\right) \quad (6)$$

where ρ is a constant set equal 0.05 and λ is the weight vector.

In-silico generation of noisy experiment results. Our group has dedicated the past five years to the extensive development of kinetic models, focusing on flow chemistry reactions. Throughout this period, we have constructed and validated a comprehensive collection of kinetic models, drawing upon a vast array of experimental data. In the present study, we have selected two models[27, 28] from our repository and incorporated an additional model developed by the Lapkin group[29] to simulate experimental outcomes.

The predetermined pre-exponential factors (A) and activation energies (E_a) of each kinetic model were used to calculate rate constants via the Arrhenius equation (Eq. 7).

$$k = Ae^{-\frac{Ea}{RT}} \tag{7}$$

where k is the rate constant, R is the molar gas constant, T is the thermodynamic temperature.

Under the new reaction conditions recommended by the acquisition function, the concentration of each reaction component was obtained by solving the reaction rate equations (Eq. 8) using the ordinary differential equation solver of SciPy.

$$\frac{dC_2}{dt} = -kC_1^{\alpha}C_2^{\beta} - kC_2^{\gamma}C_3^{\delta} \tag{8}$$

where C_1 and C_2 are the concentration of the reaction material, C_3 is the main product concentration. α, β, γ and δ stand for reaction orders

Subsequently, Gaussian noise in the form of standard deviation was added into these concentrations (Eq. 9).

$$f(x') = f(x) + f(x)\varepsilon \tag{9}$$

where $f(x')$ is the objective function with noise, ε is the experimental noise, which conforms to the Gaussian distribution[4]. The ε was taken as 0.05, 0.10, 0.15, 0.20 in this work.

Chemicals. The reactant Hexafluoropropylene oxide (C_3F_6O) was purchased from Shanghai Qinba Chemical Co., Ltd. with 98% purity, and nitrogen (99.9%) was supplied by Zhejiang Ottesen Gas Co. Al_2O_3 (≥92%) was purchased from Shanghai Maclean Biochemical Technology Co. Hydrogen (H_2, 99.999%) was purchased from Zhejiang Ottesen Gases Co., Ltd. The palladium/carbon powder catalyst (Pd/C, 10 wt %,

wetted with ca.55% water) was purchased from Anhui Zesheng Technology Co., Ltd.

Continuous flow reactor. The first experimental step in the synthesis of HFIP was the preparation of Hexafluoroacetone (HFA) from Hexafluoropropylene oxide (HFPO). As shown in Figure 1, the flow rate of the feedstock HFPO gas was controlled by a mass flow controller (Beijing Seven Star Huachuang Flowmeter Co., Ltd.). The reaction was carried out in a micro-packed bed reactor (MPBR) embedded with the catalyst of 1 g, and the MPBR and two coils were immersed in an oil bath to control the reaction temperature.

The second step of the experiment was the preparation of HFIP from HFA gas, again in an MPBR with catalyst (Pd/C, 10 wt.%, wetted with ca.55% water, filling volume of 1g), which was heated in an oil bath. A three-way valve was installed at the beginning of the unit, with one end connected to the previous reaction and the other to hydrogen. A three-way valve was also installed at the end, connected to a gas absorption device at one end and a gas sampling unit at the other. All MPBRs were made of 316 L stainless steel and had an inner diameter of 4.6 mm and a length of 15 cm.

The feedstock HFPO was delivered to the first reactor section at a predetermined flow rate. When the system reached a steady state (three times the residence time), the first three-way valve was opened and the gases from the first reactor step were delivered to the second reactor section along with the hydrogen gas at a predetermined flow rate. Sampling began once the system reached a steady state. Once sampling was complete,

the temperature control equipment was turned off and nitrogen was introduced into the reactor to remove residual feedstock and hydrogen and to ensure that the catalyst was in a nitrogen environment, thereby protecting its activity.

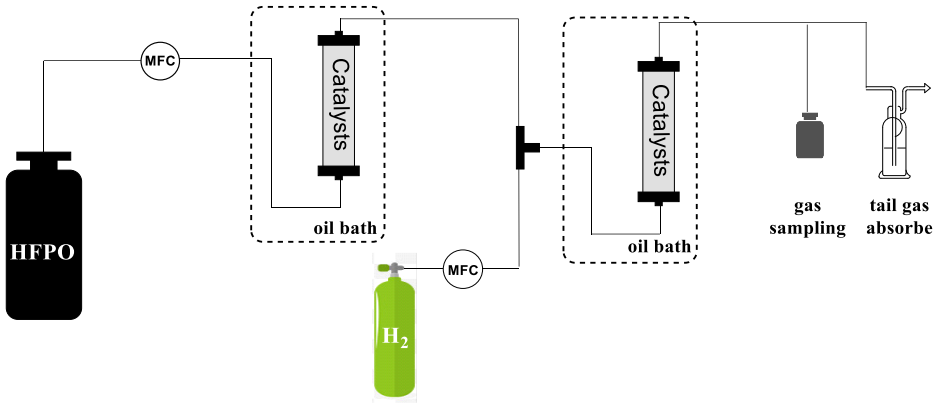

Figure 1. Overview of the continuous flow system for the telescoped synthesis of HFIP.

Sample preparation. Gases were collected from the outlet of the final reactor at a predetermined time using A gas sampling bag (Dalian Delin Gas Packaging Co., TD-401-0.005) (Fig. 1). Before each GC analysis, the gas was extracted from the sampling bag and then injected into the GC using a gas-tight needle. The gas extraction and analysis were repeated three times for each sampling bag.

Sample Analysis. The samples were measured by a Gas Chromatograph (GC) (Foley 9790plus). Measurement conditions were as follows: column type: HP-INNOWAX (30m × 0.25 mm × 0.5μm), column temperature was maintained at 80 ℃ for 5 min and then ramped up to 200 ℃ at a rate of 10 ℃/min. The inlet temperature was 250 ℃. The FID detector temperature was 250 ℃. The airflow rate was 300 mL/min. The hydrogen flow rate was 30 mL/min, and the carrier gas (N_2) flow rate was 0.8 mL/min. The normalized peak areas (NPA, %) obtained from the GC chromatograms were used to calculate the conversion (C) as shown in Eq. 10[30].

$$C = \frac{A_{HFPO0} - A_{HFPOt}}{A_{HFPO0}} \quad (10)$$

where A_{HFPO0} and A_{HFPOt}, represent the normalized peak areas of pre-reaction HFPO and post-reaction HFPO.

The E-factor is defined as the ratio of the mass of waste to product (Eq. 11)[8].

$$E - \text{factor} = \frac{m_{waste}}{m_{product}} \quad (11)$$

where $m_{product}$, m_{waste} represent the mass of the product and the waste.

Results and Discussion

In-silico comparison of the noise-handling capability of different MOBO acquisition functions. The first part of this study is to investigate the noise-handling capability of four MOBO acquisition functions by comparing their performance in chemical reactions under different noise levels. Since it is difficult to control the noise level in wet lab experiments, kinetic models were used to simulate noisy experimental results. We chose three reactions with known kinetic models (Scheme 1), including the condensation amidation of piperazine with benzoic acid[31] (Case 1), the nucleophilic aromatic substitution between 2,4-difluoronitrobenzene and morpholine[29] (Case 2), and the monoacylation reaction of m-phenylenediamine and benzoic anhydride[27] (Case 3).

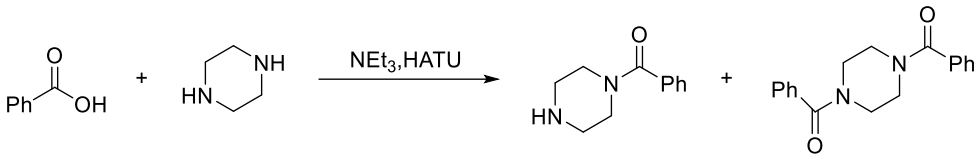

1 2 3 4

Case 1. Condensation amidation of piperazine with benzoic acid.

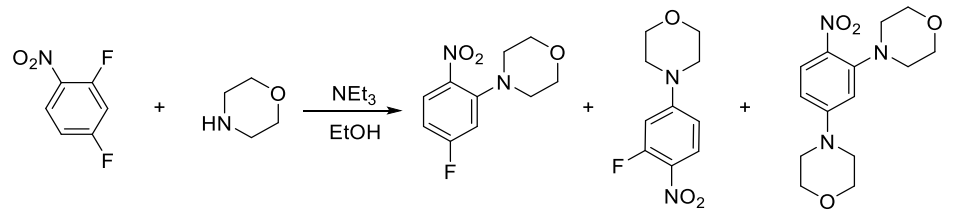

5 6 7 8 9

Case 2. S_NAr reaction.

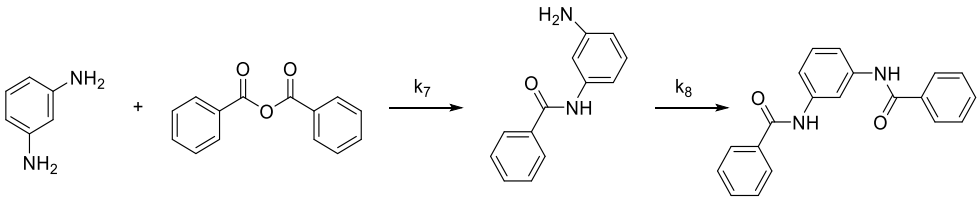

10 11 12 13

Case 3. Continuous flow monoacylation reaction

Case	1	2	3
Variables	Temperature (-30-70 ℃) Residence time (30-120 s) Con. of **1** (10-200 mM) HAUT (10-200 mM) Con. of **2** (10-200 mM)	Temperature (30-120 ℃) Residence time (30-120 s) Con. of **5** (0.1-0.5 M) equivalents of **6** (1.0–5.0)	Temperature (30-120 ℃) Residence time (30-120 s) Con. of **11** (0.1-0.5 M) equivalents of **10** (1.0–3.0)
Objectives	Yield and E-factor		

Scheme 1. Three cases and their optimization variables and goals

The workflow for performing MOBO based on kinetic model simulators using the FlowBO platform is shown in Figure 2. FlowBO is a Bayesian Optimization platform for flow chemistry that was first developed in our previous work[20]. In this study, FlowBO was added with three different acquisition functions: qNEHVI, qEHVI, and qNParEGO. Also, the well-recognized open-source MOBO platform TSEMO[8] was used as a benchmark (comparison with three acquisition functions based on Gaussian

processes). In this workflow, the user first identified the variables and objectives to be optimized (Scheme 1, lower part). The initial set of experimental variables was then sampled by Latin Hypercube Sampling (LHS)[29] and fed into the kinetic model simulator, and the corresponding results were used for the initial training of the surrogate model. Based on the trained surrogate model, the MOBO acquisition function proposed new experimental variable settings, and the kinetic model simulator generated the corresponding experimental results. After adding the newly generated results to the training dataset, the next iteration started with updating the surrogate model using the updated training dataset. This iteration continued until a predetermined maximum number of experiments was reached. This workflow was conducted independently for each MOBO acquisition function.

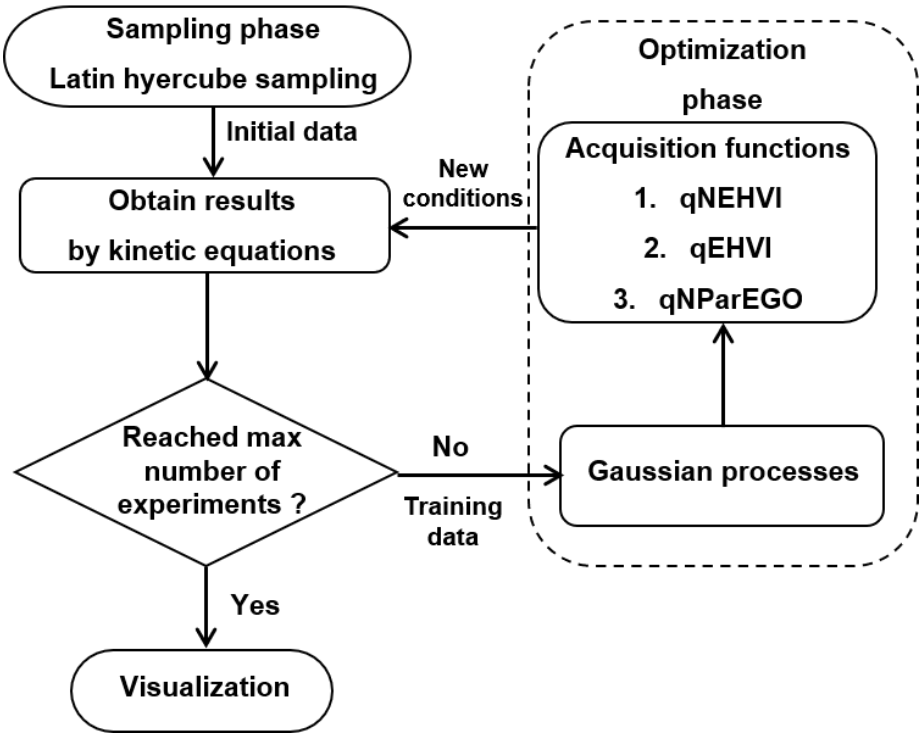

Figure 2. The workflow of using FlowBO to perform multi-objective Bayesian optimization (MOBO) based on kinetic model simulators

The hypervolume was calculated after each Bayesian optimization iteration (Figure 3). A larger hypervolume means an improved Pareto front that leads to better multi-objective optimization. The results show that qNEHVI significantly outperforms other MOBO acquisition functions in both the final hypervolume and the initial rate of hypervolume increase in the high-noise cases (15% and 20%) of Case 2 and Case 3. In contrast, the benchmark TSEMO did not perform well in both cases at a 10% noise level or higher, whose hypervolume growth was significantly hindered by increased noise. On the other hand, in Case 1, the final hypervolume of all the algorithms is comparable, implying that this reaction's optimization was not significantly affected by noise, probably due to the relative simplicity of its reaction mechanism. As described in the original work on this algorithm, qNEHVI maintains one-step Bayesian optimality in noisy environments by integrating over the uncertainty of the function values at the observed points[21], which allows it to identify well-distributed Pareto fronts under highly noisy observations. Furthermore, our observations show that qNEHVI and qEHVI perform similarly in all cases under lower noise (5%) conditions, which is consistent with the literature claim that both algorithms perform equally well in experiments when no noise is introduced[21].

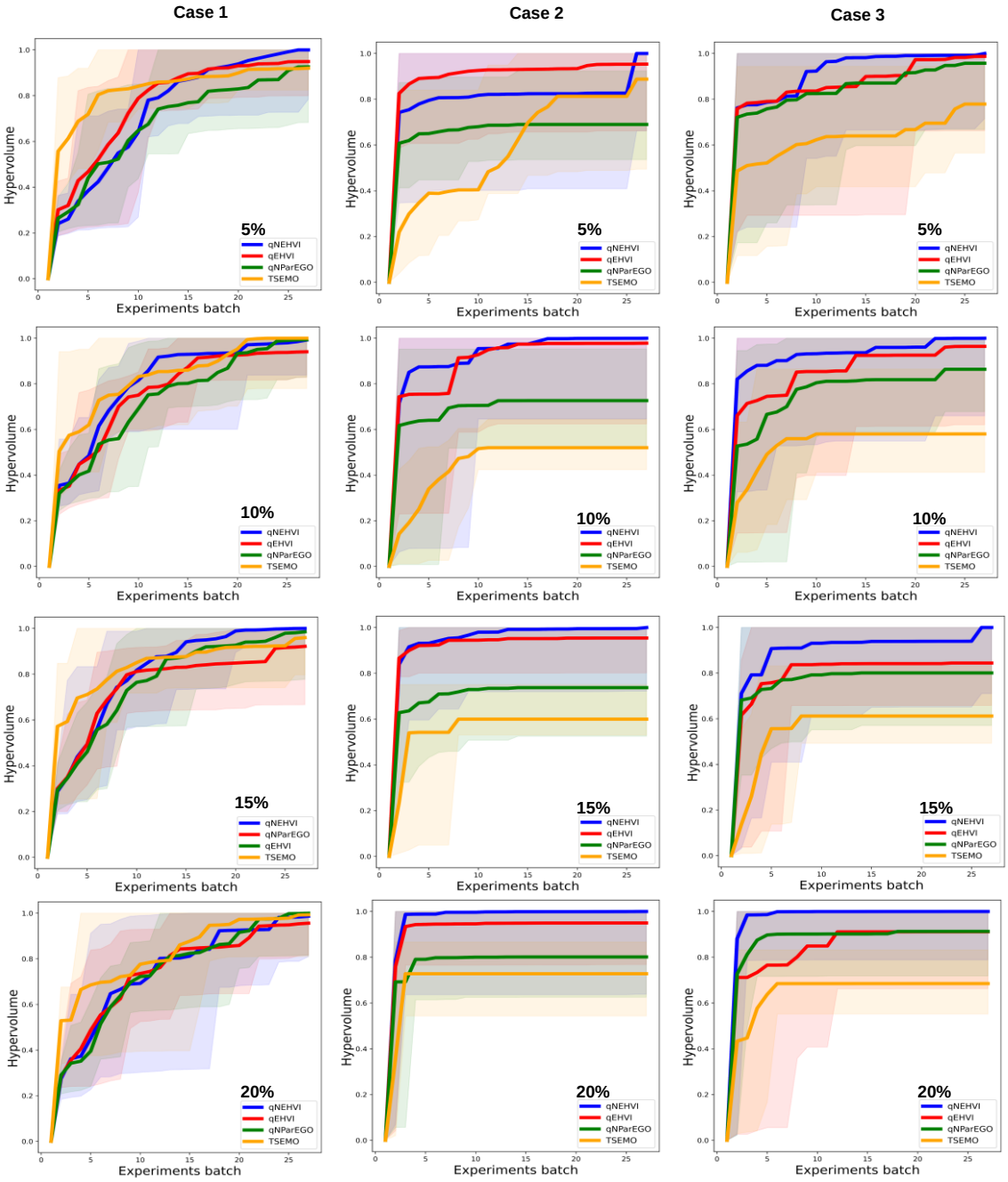

Figure 3. Plots showing the average change in hypervolume across 10 runs with 25 function evaluations each. The shaded area is the upper and lower limits

In addition, the mean computational time required for each MOBO acquisition function was analyzed (Table 1). The results show that it required the longest time to compute TSEMO, which has a time-consuming multi-objective genetic algorithm (NSGA-II)[25].

In contrast, *q*NEHVI was the fastest to compute as the method has a second-order gradient algorithm (L-BFGS-B) with random restarts[32]. In addition, all three MOBO acquisition functions embedded in FlowBO, including qNEHVI, qEHVI, and qNParEGO, were implemented based on the BoTorch framework with GPU acceleration[33].

Table 1. Mean computational time of the MOBO models in each case

Case	Computational time (min)			
	qNEHVI	**qEHVI**	**qNParEGO**	**TSEMO**
1	1.14	1.24	0.84	3.02
2	0.98	0.81	1.20	3.24
3	1.21	1.40	0.90	3.05

Our previous work has successfully used qNEHVI as a MOBO acquisition function algorithm for the multi-objective optimization of a one-step heterogeneous catalysis reaction[30]. Near the end of this study, we noticed that the Lapkin group reported a better optimization of qNEHVI than TSEMO for the MOBO of the Schotten-Baumann reaction, both in terms of hypervolume improvement and computational time[32], which is also consistent with our findings in this study.

Performing MOBO for a two-step heterogeneous catalysis in continuous flow. Based on the results of Part 1, we decided to use qNEHVI as the MOBO acquisition function for telescoped flow synthesis of hexafluoroisopropanol (Figure 4). The aim of the optimization was to maximize the conversion while minimizing the E-factor (total waste produced by the process/total products)[34].

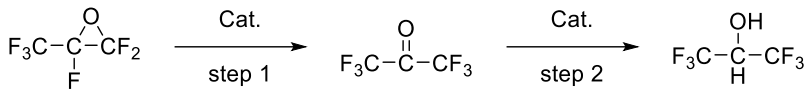

Figure 4. Multi-step synthesis of HFIP from HFPO

The ranges of decision variables are shown in Table 2. The ranges of gas flow rates of HFPO and hydrogen were determined by the limits of the mass flow controller. In addition, the upper limit for T_1 (the temperature for the first step reaction) was set to 120℃ because HFPO tends to decompose at temperatures above 150 ℃[35]. The upper limit for T_2 (the temperature for the second step reaction) was set to 170 ℃ for the safety of the tubular reactor.

Table 2. Lower and upper bounds for decision variables in optimization

Range [a]	F_{HFPO} (ml/min)	T_1 (℃)	$F_{hydrogen}$ (ml/min)	T_2 (℃)
Lower	5	35	5	35
Upper	45	120	100	170

a. The temperature of the first reaction step (T_1), the flow rate of hydrogen ($F_{hydrogen}$), the temperature of the second reaction step (T_2), and the flow rate of hexafluoropropylene oxide (F_{HFPO}) .

The main difference between the MOBO in Part 1 and Part 2 was that the experiment results in Part 2 were derived from wet lab experiments instead of the simulator (Figure 5). During the sampling phase, the LHS sampled ten sets of experimental conditions, and their corresponding experimental results were used as the initial training dataset. The surrogate model (Gaussian Process) was then trained on this dataset, after which the qNEHVI recommended a new set of experimental conditions (temperature, flow rate, etc.). Experimental data from the new experiments were added to the training dataset for a new round of surrogate model training and qNEHVI recommendation. The optimization stopped after ten rounds of iterations.

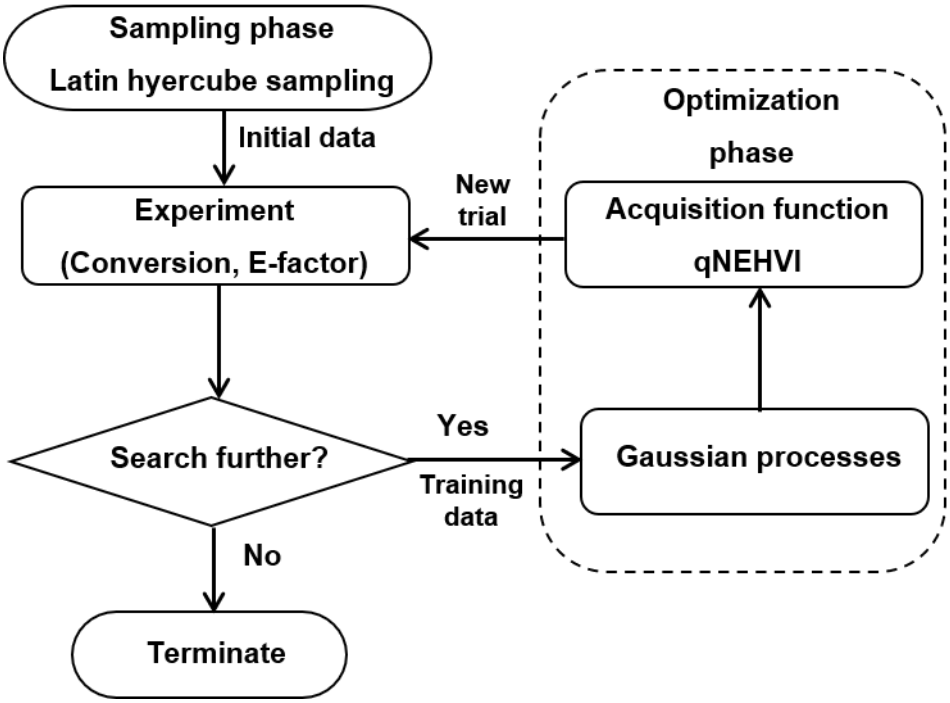

Figure 5. Multi-objective Bayesian optimization (MOBO) with wet lab experiments. The iterative process was repeated until the conversion rate and environmental factors reached a satisfactory compromise.

The optimization results are shown in Figure 6a. The black symbol x represents the ten data points in the initial sampling phase, and the color represents the number of iterations in the optimization phase. A maximum conversion rate of 76.20% and a minimum E-factor of 0.3744 were found in Iteration 9 of the optimization phase. Figure 6b shows the effect of each variable on the two objectives. As the ratio of $F_{hydrogen}$ and F_{HFPO} decreased, the conversion rate increased significantly. On the contrary, when this ratio was too large, the conversion rate decreased slightly and the E-factor increased, possibly due to the insufficient contact between the reactants and the catalysts. In addition, the increase in T_2 significantly increased the conversion rate.

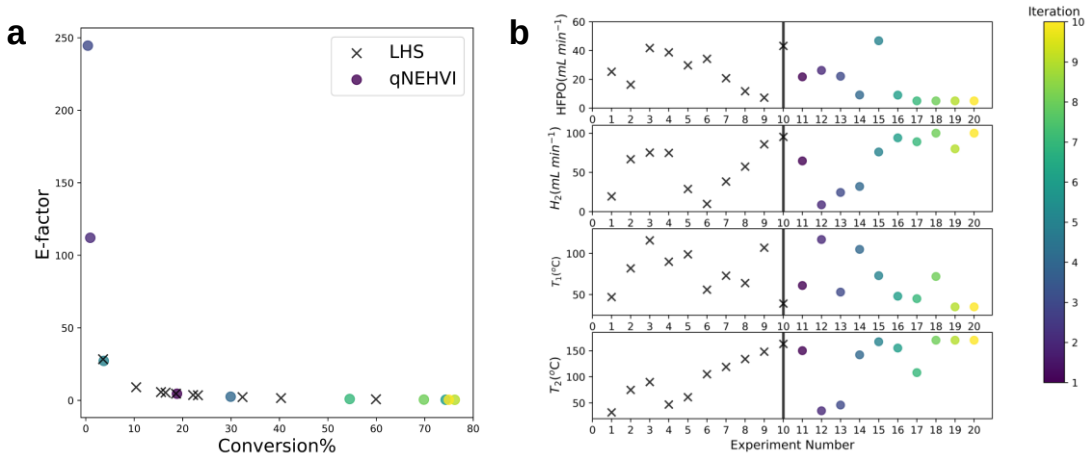

Figure 6. Experimental results of multi-objective optimization a) E-factor and Conversion. b) Exploration of four decision variables. The symbol X represents the 10 initial samples of LHS and the color represents the number of iterations in the acquisition function suggestions.

Table 3 lists the corresponding experimental conditions in Figure 6. We noted that the optimization searched for experimental conditions close to the optimal result, such as Iterations 6 and 10 suggested in the optimization phase. On the other hand, the algorithm also searched in relatively unfamiliar sampling space (e.g., Iterations 2 and 4 in the optimization phase), significantly different from the variable combinations in the sampling phase. These phenomena suggest that the qNEHVI algorithm maintains a good balance between exploitation and exploration - while exploitation tries to improve the current optimum, exploration is essential to avoid falling into local optima.

Table 3. Combination of variables explored by Bayesian optimization with data sampled by LHS and acquisition function.

Sampled By	Entries/Iterations	F_{HFPO} (ml/min)	T_1 (°C)	$F_{hydrogen}$ (ml/min)	T_2 (°C)	Conversion	E-factor
LHS (sampling phase)	1	25.25	47	19.40	32	15.52	5.742
	2	16.25	82	66.80	75	32.36	2.234
	3	41.75	116	75.30	90	22.16	3.722
	4	38.75	90	47.80	47	10.39	9.071
	5	29.75	99	28.80	61	18.62	4.620
	6	34.25	56	9.80	105	3.560	28.39
	7	20.75	73	38.30	119	16.47	5.354
	8	11.75	64	57.30	134	59.91	0.7470
	9	7.25	107	85.80	148	40.31	1.597
	10	43.25	39	95.30	163	23.15	3.520
Acquisition-function (optimization phase)	1	21.70	61	64.60	150	18.83	4.558
	2	26.20	117	8.60	35.0	0.925	112.1
	3	22.10	53	24.40	46.0	0.426	244.6
	4	9.10	105	32.00	142	29.92	2.4978
	5	46.80	73	76.00	167	3.712	27.19
	6	9.00	48	94.00	155	74.32	0.4087
	7	5.00	45	89.00	108	54.5	0.9218
	8	5.00	72	100.00	170	69.82	0.5003
	9	5.00	35	80.00	170	76.20	0.3744
	10	5.00	35	100.00	170	74.97	0.3972

Conclusion

In this work, we first developed an in-silico platform to rapidly screen MOBO methods and then performed wet-lab experiments to validate the selected MOBO method. In the in-silico platform FlowBO, we generate noisy experimental results using a reaction simulator based on kinetic modeling and compared the noise-handling ability of four MOBO acquisition functions in the MOBO of three different reactions. qNEHVI performed the best in high-noise environments and had the shortest time to find the optimal solution. In wet-lab experiments, we applied qNEHVI to the MOBO of the telescoped heterogeneous synthesis of HFIP. Experimental results show that qNEHVI

can quickly find a compromise for the conversion and E-factor within an acceptable number of trials. In future work, we will aim to embed telescoped reaction simulators on the FlowBO platform for MOBO method screening in more difficult tasks. In addition, we will test telescoped catalysis involving more than two steps or in combination with separation processes to further demonstrate and improve MOBO methods.

Supplementary Material

The Supplementary Material provides the following content:

1. Kinetic equations for Scheme 1;
2. Numerical values for Figure 3;
3. NMR spectra and HRMS data.

Acknowledgments

This research was supported by Zhejiang Province Science and Technology Plan Project under Grant No. 2022C01179 and the Joint Funds of the Zhejiang Provincial Natural Science Foundation of China under Grant No. LHDMZ23B060001.

References

1. Taylor CJ, Pomberger A, Felton KC, Grainger R, Barecka M, Chamberlain TW, Bourne RA, Johnson CN, Lapkin AA. A Brief Introduction to Chemical Reaction Optimization. Chem Rev. 2023;123(6):3089-3126.
2. Häse F, Roch LM, Kreisbeck C, Aspuru-Guzik A. Phoenics: A Bayesian Optimizer for Chemistry. ACS Cent Sci. 2018;4(9):1134-1145.

3. Tachibana R, Zhang K, Zou Z, Burgener S, Ward TR. A Customized Bayesian Algorithm to Optimize Enzyme-Catalyzed Reactions. ACS Sustain Chem Eng. 2023;11(33):12336-12344.
4. Ruan Y, Lin S, Mo Y. AROPS: A Framework of Automated Reaction Optimization with Parallelized Scheduling. J Chem Inf Model. 2023;63(3):770-781.
5. Liang R, Duan X, Zhang J, Yuan Z. Bayesian based reaction optimization for complex continuous gas–liquid–solid reactions. React Chem Eng. 2022;7(3):590-598.
6. Shields BJ, Stevens J, Li J, Parasram M, Damani F, Alvarado JIM, Janey JM, Adams RP, Doyle AG. Bayesian reaction optimization as a tool for chemical synthesis. Nature. 2021;590(7844):89-96.
7. Wang Y, Chen TY, Vlachos DG. NEXTorch: A Design and Bayesian Optimization Toolkit for Chemical Sciences and Engineering. J Chem Inf Model. 2021;61(11):5312-5319.
8. Schweidtmann AM, Clayton AD, Holmes N, Bradford E, Bourne RA, Lapkin AA. Machine learning meets continuous flow chemistry: Automated optimization towards the Pareto front of multiple objectives. Chem Eng J. 2018;352:277-282.
9. Torres JAG, Lau SH, Anchuri P, Stevens JM, Tabora JE, Li J, Borovika A, Adams RP, Doyle AG. A Multi-Objective Active Learning Platform and Web App for Reaction Optimization. J Am Chem Soc. 2022;144(43):19999-20007.
10. Kershaw OJ, Clayton AD, Manson JA, Barthelme A, Pavey J, Peach P, Mustakis J, Howard RM, Chamberlain TW, Warren NJ, Bourne RA. Machine learning

directed multi-objective optimization of mixed variable chemical systems. Chem Eng J. 2023;451.

11. Dunlap JH, Ethier JG, Putnam-Neeb AA, Iyer S, Luo S-XL, Feng H, Garrido Torres JA, Doyle AG, Swager TM, Vaia RA, Mirau P, Crouse CA, Baldwin LA. Continuous flow synthesis of pyridinium salts accelerated by multi-objective Bayesian optimization with active learning. Chem Sci. 2023;14(30):8061-8069.
12. Nambiar AMK, Breen CP, Hart T, Kulesza T, Jamison TF, Jensen KF. Bayesian Optimization of Computer-Proposed Multistep Synthetic Routes on an Automated Robotic Flow Platform. ACS Cent Sci. 2022;8(6):825-836.
13. Clayton AD, Pyzer-Knapp EO, Purdie M, Jones MF, Barthelme A, Pavey J, Kapur N, Chamberlain TW, Blacker AJ, Bourne RA. Bayesian Self-Optimization for Telescoped Continuous Flow Synthesis. Angew Chem Int Ed Engl. 2023;62(3):e202214511.
14. Jorayev P, Russo D, Tibbetts JD, Schweidtmann AM, Deutsch P, Bull SD, Lapkin AA. Multi-objective Bayesian optimisation of a two-step synthesis of p-cymene from crude sulphate turpentine. Chem Eng Sci. 2022;247.
15. Sagmeister P, Ort FF, Jusner CE, Hebrault D, Tampone T, Buono FG, Williams JD, Kappe CO. Autonomous Multi-Step and Multi-Objective Optimization Facilitated by Real-Time Process Analytics. Adv Sci. 2022;9(10):2105547.
16. Zhokh OO, Trypolskyi AI, Strizhak PE. Discrimination of a chemical kinetic mechanism for heterogeneously catalyzed reactions using intraparticle diffusion. Chem Eng J. 2023;474.

17. Xue HT, Qi TT, Su WK, Wu KJ, Su A. Heterogeneous Continuous Flow Hydrogenation of Hexafluoroacetone Trihydrate and Its Kinetic Modeling. Ind Eng Chem Res. 2023;62(15):6121-6129.
18. Chen JL, Lin XY, Xu F, Chai KJ, Ren MN, Yu ZQ, Su WK, Liu FF. An Efficient Continuous Flow Synthesis for the Preparation of N-Arylhydroxylamines: Via a DMAP-Mediated Hydrogenation Process. Molecules. 2023;28(7).
19. Diwale S, Eisner MK, Carpenter C, Sun W, Rutledge GC, Braatz RD. Bayesian optimization for material discovery processes with noise. Mol Syst Des Eng. 2022;7(6):622-636.
20. Luo GH, Yang XL, Qi TT, Xu QL, Su WK, Su A. FlowBO: A Flow Chemistry Bayesian Optimization Framework Benchmarked by Kinetic Models. ChemRxiv. 2023.
21. Daulton S, Balandat M, Bakshy E. Parallel bayesian optimization of multiple noisy objectives with expected hypervolume improvement. NIPS. 2021;34:2187-2200.
22. Snoek J, Larochelle H, Adams RP. Practical Bayesian Optimization of Machine Learning Algorithms. NIPS. 2012;4:2951-2959.
23. Leonenko N, Malyarenko A. Matérn Class Tensor-Valued Random Fields and Beyond. J Stat Phys. 2017;168(6):1276-1301.
24. Emmerich MTM, Giannakoglou KC, Naujoks B. Single- and multiobjective evolutionary optimization assisted by Gaussian random field metamodels. IEEE Trans Evol Comput. 2006;10(4):421-439.
25. Bradford E, Schweidtmann AM, Lapkin A. Efficient multiobjective optimization

employing Gaussian processes, spectral sampling and a genetic algorithm. J Global Optim. 2018;71(2):407-438.

26. Knowles J. ParEGO: a hybrid algorithm with on-line landscape approximation for expensive multiobjective optimization problems. IEEE Trans Evol Comput. 2006;10(1):50-66.

27. Xu QL, Fan HC, Yao HM, Wang DH, Yu HW, Chen BB, Yu ZQ, Su WK. Understanding monoacylation of symmetrical diamines: A kinetic study of acylation reaction of m-phenylenediamine and benzoic anhydride in microreactor. Chem Eng J. 2020;398.

28. Xu QL, Liu JM, Yao HM, Zhao JY, Wang ZK, Liu JL, Zhou JD, Yu ZQ, Su WK. Insight into Fundamental Rules of Phenylenediamines Selective Monoacylation by the Comparisons of Kinetic Characteristics in Microreactor. Bull Korean Chem Soc. 2021;42(10):1336-1344.

29. Felton KC, Rittig JG, Lapkin AA. Summit: Benchmarking Machine Learning Methods for Reaction Optimisation. Chemistry–Methods. 2021;1(2):116-122.

30. Qi TT, Luo GH, Xue HT, Su F, Chen JL, Su WK, Wu K-J, Su A. Continuous heterogeneous synthesis of hexafluoroacetone and its machine learning-assisted optimization. J Flow Chem. 2023;13(3):337-346.

31. Xu QL, Zhang SQ, Zhao JY, Wang ZK, Liu LC, Zhou PC, Yu ZQ, Su WK. Improving the reaction efficiency of condensation amidation of piperazine with benzoic acid based on kinetics study in microreactors. J Flow Chem. 2021;11(4):855-866.

32. Zhang J, Sugisawa N, Felton KC, Fuse S, Lapkin AA. Multi-objective Bayesian optimisation using q-noisy expected hypervolume improvement (qNEHVI) for the Schotten–Baumann reaction. React Chem Eng. 2024.

33. Balandat M, Karrer B, Jiang DR, Daulton S, Letham B, Wilson AG, Bakshy E. BOTORCH: A Framework for Efficient Monte-Carlo Bayesian Optimization. NIPS. 2020;33:21524-21538.

34. Tieves F, Tonin F, Fernández-Fueyo E, Robbins JM, Bommarius B, Bommarius AS, Alcalde M, Hollmann F. Energising the E-factor: The E+-factor. Tetrahedron. 2019;75(10):1311-1314.

35. Millauer H, Schwertfeger W, Siegemund G. Hexafluorpropenoxid – eine Schlüsselverbindung der organischen Fluorchemie. Angew Chem. 1985;97(3):164-182.